Balancing Structure and Performance: Optimized BZO Nanorod Doping in Ca-Interlayered YBCO Multilayers

C. Condo, S. Mejia, M. M. Aye, E. Rivasto, H. Huhtinen, and P. Paturi

***Abstract*—This study demonstrates the enhancement of critical current density over a wide temperature and magnetic field range in BZO-doped YBCO multilayer structures using a Ca-doped YBCO intermediate layer. Compared to single-layer BZO-doped YBCO films, the Ca-doped interlayer improves crystalline quality and reduces non-uniform strain, particularly at low BZO doping concentrations, and promotes better growth of BZO nanorods. Additionally, multilayering slightly increases YBCO's oxygen content across all BZO concentrations, contributing to a higher critical temperature and zero-field critical current density. Besides of this, multilayering enhances critical current density across the magnetic field range, especially at low fields and high BZO concentrations. However, the highest absolute zero-field critical current density is achieved in undoped multilayered YBCO, whereas in fields above 2 T and up to 50 K, the best performance is obtained with 4% BZO-doped YBCO layers separated by Ca-doped interlayers. At around 1 T, 2% BZO doping yields the highest critical current density. This paper also explores the possible mechanisms behind these effects, proposing that multilayering BZO-doped YBCO with a crystal structure-balancing interlayer could be key to next-generation YBCO coated conductors for high-temperature superconductor applications. Optimising the BZO concentration is crucial when tailoring YBCO compositions for different operating conditions.**

***Index Terms*—HTS, YBCO, Ca-doped YBCO, multilayers, crystalline quality, flux pinning, critical current density.**

I. Introduction

THE high temperature superconductor $YBa_2Cu_3O_{6+x}$ (YBCO) is widely used in the development of second-generation coated conductors, flexible, high-performance tapes that serve as the foundational components for numerous advanced applications, including high-field magnets for future fusion reactors, rotating machines, and energy storage systems [1], [2], [3]. The ability of these coated conductors to carry large currents in strong magnetic fields is critical to their performance and commercial viability.

Received 7 October 2025; revised 18 December 2025; accepted 14 January 2026. Date of publication 20 January 2026; date of current version 12 February 2026. This work was supported by Jenny and Antti Wihuri Foundation. *(Corresponding author: H. Huhtinen.)*

C. Condo, S. Mejia, M. M. Aye, H. Huhtinen, and P. Paturi are with the Wihuri Physical Laboratory, Department of Physics and Astronomy, University of Turku, FI-20014 Turku, Finland (e-mail: hannu.huhtinen@utu.fi).

E. Rivasto is with the Wihuri Physical Laboratory, Department of Physics and Astronomy, University of Turku, FI-20014 Turku, Finland, and also with the CP3-Origins, University of Southern Denmark, 5230 Odense, Denmark.

Color versions of one or more figures in this article are available at https://doi.org/10.1109/TASC.2026.3656256.

Digital Object Identifier 10.1109/TASC.2026.3656256

One of the most effective strategies for enhancing in-field performance is the introduction of artificial pinning centers, particularly through doping YBCO with $BaZrO_3$ (BZO). During film growth, BZO self-assembles into vertically aligned nanorods that penetrate the YBCO matrix, significantly improving flux pinning and increasing the critical current density (J_c) under applied magnetic fields [4], [5], [6], [7], [8], [9]. However, high BZO concentrations can induce strain and microstructural imperfections, leading to reduced crystalline quality and a drop in zero-field $J_c(0)$ [10], [11], [12], [13].

To mitigate these issues, this work explores a multilayered architecture, where differently BZO-doped YBCO layers are alternated with Ca-doped YBCO interlayers [14], [15], [16], [17]. These intermediate layers act as structural buffers, relaxing accumulated strain, compensating for oxygen deficiencies, and promoting higher-quality epitaxial growth. As a result, both the zero-field and in-field J_c are enhanced across a broad range of temperatures and magnetic fields [18], [19], [20], [21]. This study demonstrates that combining the optimal BZO nanorod doping concentration with Ca-doped multilayering offers a robust pathway to optimizing the structural and superconducting properties of YBCO films. The approach provides a promising route toward next-generation coated conductors tailored for high-performance applications in strong magnetic field environments.

II. Experimental Details

Multilayer YBCO films incorporating $BaZrO_3$ (BZO) at concentrations ranging from 0 wt.% to 10 wt.% in 2 wt.% increments (designated as M0, M2, M4, M6, M8, and M10) were fabricated with 30% Ca-doped YBCO spacer layers ($Y_{0.7}Ca_{0.3}Ba_2Cu_3O_{6+x}$) using pulsed laser deposition (PLD) on $SrTiO_3$ (STO) substrates, as illustrated with layer thicknesses in Fig. 1 [20], [22]. The films were deposited at 750 °C using a KrF excimer laser ($\lambda = 248$ nm) operated at a repetition rate of 5 Hz and a laser fluence of 1.3 J cm^{-2} under an oxygen pressure of 0.175 Torr. After deposition, the films were post-annealed *in situ* at 725 °C in 1 atm of oxygen for 10 min. For comparison, single-layer films with identical BZO concentrations (labelled S0, S2, S4, S6, S8, and S10) were also prepared under the same conditions.

Crystallographic characterization was carried out using a PANalytical Empyrean x-ray diffractometer operating in

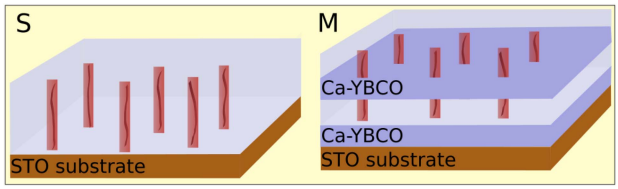

Fig. 1. Schematic illustration showing the structural differences between a single-layer S (a) and a multilayer M (b) YBCO film deposited on STO substrates, where BZO forms nanorods penetrating through the layer. In the multilayer samples, two ≈170 nm thick 4BZO layers were grown on top of ≈30 nm thick 30% Ca-doped YBCO layers. The total thickness of the single-layer films is ≈350 nm, regardless of the BZO concentration.

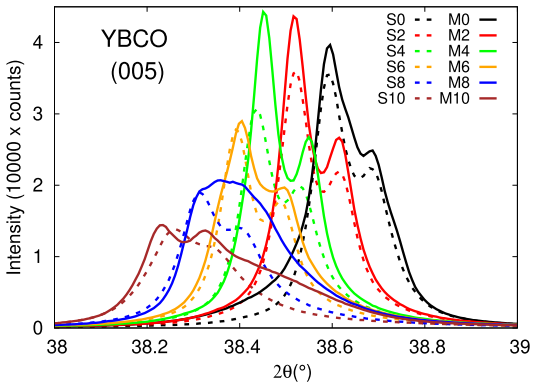

Fig. 2. Evolution of the Cu $K_{\alpha 1/\alpha 2}$ XRD 2θ (005) peak pairs in single-layer (solid lines) and multilayer (dashed lines) YBCO films with varying BZO dopant concentrations.

TABLE I
STRUCTURAL DIFFERENCES OF SINGLE-LAYER AND MULTILAYER YBCO FILMS WITH VARYING BZO CONCENTRATIONS, AS DETERMINED BY XRD.

Sample	c(Å)	$\Delta\theta(^\circ)$	$\Delta\phi(^\circ)$	$\Delta\omega(^\circ)$	$\varepsilon_{\mathrm{WH}}(\%)$	I_{ratio}
S0	11.65	0.10	1.92	0.32	0.092	14.5
S2	11.68	0.09	1.89	0.30	0.093	14.9
S4	11.70	0.10	1.92	0.31	0.104	14.4
S6	11.71	0.10	1.94	0.30	0.099	14.1
S8	11.73	0.13	1.93	0.49	0.154	14.2
S10	11.75	0.18	2.08	0.70	0.224	14.3
M0	11.65	0.11	1.94	0.30	0.098	12.4
M2	11.68	0.09	1.86	0.27	0.088	14.0
M4	11.70	0.08	1.86	0.29	0.094	13.7
M6	11.71	0.12	1.89	0.27	0.151	13.3
M8	11.72	0.20	1.87	0.29	0.269	12.7
M10	11.74	0.33	1.92	0.31	0.443	12.8

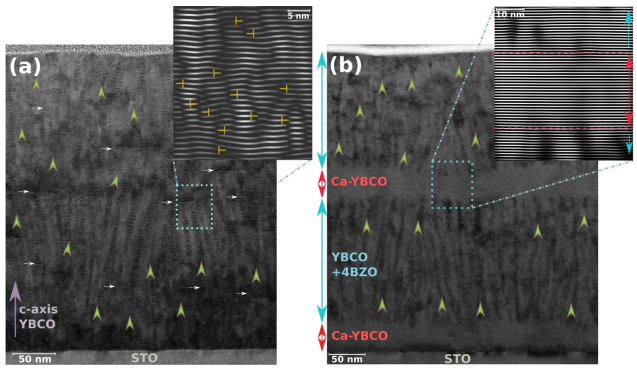

Fig. 3. Cross-sectional TEM images of (a) single-layer S4BZO and (b) multilayer M4BZO films. BZO nanorods (green arrowheads), stacking faults (white arrows), and dislocations (yellow markers) are identified. Insets show inverse FFT enlargements of marked regions, highlighting structural differences.

Bragg–Brentano geometry. High-resolution transmission electron microscopy (HRTEM) was performed with a JEOL JEM-2200FS microscope equipped with a 200 kV field emission gun (FEG) and an in-column Omega energy filter. Magnetic characterization was carried out using a Quantum Design Physical Property Measurement System (PPMS) magnetometer. (J_c) was extracted from the opening of the magnetization hysteresis loops, applying the Bean model for rectangular thin films [23].

III. Results and Discussion

A. Effect of Ca-Doped Spacer Layer in Crystalline Quality

Comprehensive XRD characterization, including θ–2θ, ω, and 2D (θ–ϕ) scans, was carried out to assess the crystalline phase composition, identify potential impurities, and evaluate both in-plane and out-of-plane structural quality. As illustrated in Fig. 2, increasing the BZO concentration results in broadening and systematic shift of the 2θ peaks towards lower angles, which suggests the presence of enhanced microstrain and uniform lattice strain [24], [25]. These observations are consistent with the elongation of the out-of-plane lattice parameter c, as detailed in Table I. Moreover, the significantly higher diffraction peak intensities observed in the multilayer samples, compared to their single-layer counterparts, imply that the intermediate Ca-doped YBCO layer promotes improved epitaxial growth, thereby enhancing the overall crystalline quality. This beneficial effect of multilayering is further supported by the narrower peak widths observed in both the ϕ- and ω-scan directions, particularly at higher BZO concentrations (Table I). We also determined the microstrain values, $\varepsilon_{\mathrm{WH}}$, from Williamson–Hall analysis [25]. The results show that, with increasing BZO dopant concentration, the non-uniform microstrain remains approximately constant in both the single-layer and multilayer film series up to a BZO content of about 6%. Above this concentration, the microstrain increases rapidly, with a more pronounced increase observed in the multilayer films. Additionally, the intensity ratio of the XRD reflections $I(005)/I(004)$, I_{ratio}, is consistently lower in the multilayer films across all BZO doping levels. This trend is indicative of enhanced oxygen incorporation in the BZO-doped YBCO layers, likely due to oxygen diffusion from the underlying Ca-doped YBCO layers, as previously proposed in related studies [21], [26], [27].

TEM analysis reveals key differences in the microstructural evolution of YBCO films with embedded BZO nanorods, as shown in Fig. 3. While both the single layer S4 and multilayer M4 films contain BZO nanorods with an average diameter of 6 nm and edge-to-edge spacing of 12 nm, notable contrasts emerge in defect structures and overall ordering. In S4, the nanorods are poorly aligned, often deviating from the YBCO c-axis and showing irregular spacing. This disordered growth extends through the film thickness and is accompanied by a high

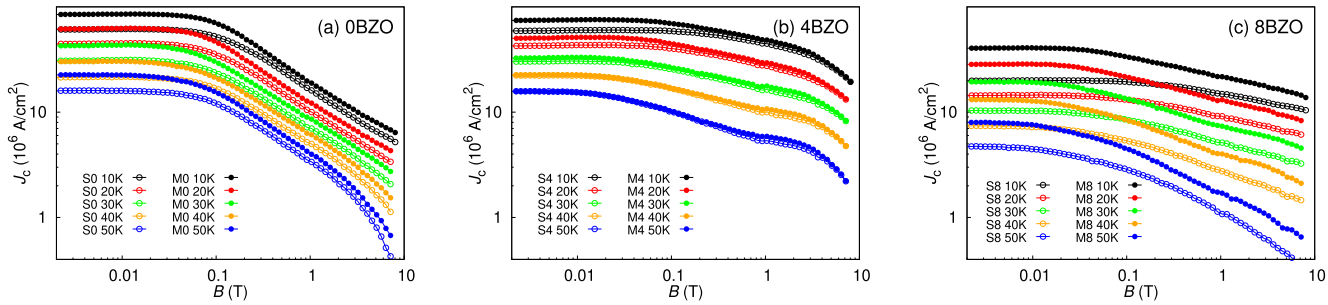

Fig. 4. Magnetic field dependence of J_c, illustrating the differences between single-layer and multilayer YBCO films across a wide range of magnetic fields and temperatures: (a) without BZO doping (0BZO), (b) with intermediate BZO doping (4BZO), and (c) with high BZO doping concentration (8BZO).

density of dislocations, stacking faults, and local strain, not limited to the YBCO/STO interface. Conversely, the M4 multilayer displays a much more ordered architecture. The BZO nanorods are well-aligned along the c-axis within each layer and grow coherently across the Ca-doped YBCO interlayers. This results in reduced defect density and improved crystallinity across the entire film. The enhanced structural quality is attributed to the periodic strain relaxation and interface smoothing provided by the Ca-doped YBCO spacers, which support uniform nucleation and guide nanorod alignment.

B. Improved Critical Current Densities by Multilayering

The temperature-dependent resistivity measurements in zero dc magnetic field (not shown) indicate that the critical temperature decreases with increasing BZO dopant concentration (from 0 to 10 wt.% BZO), similarly from ≈91 K to ≈86 K in both the single-layer and multilayer film series. However, the superconducting transition width increases over the same BZO concentration range, from <1 K to ≈9 K in the single-layer films and from <1 K to ≈6 K in the multilayer films.

Using the Bean model [23], the magnetic hysteresis loops were analyzed to derive the $J_c(B)$ dependence on applied magnetic field across a range of temperatures up to 50 K. Representative $J_c(B)$ curves for three BZO doping levels, 0BZO, 4BZO, and 8BZO, are presented in Fig. 4. A general trend is observed whereby the zero-field $J_c(0)$ decreases and the overall shape of the curves alters with increasing BZO content.

In particular, the power-law-like decrease in $J_c(B)$ observed in the undoped (0BZO) films after the initial plateau changes markedly at higher doping levels, indicating enhanced flux pinning and improved in-field performance above approximately 100 mT. In moderately BZO-doped samples, such as 4BZO and 6BZO, a noticeable enhancement in the $J_c(B)$ characteristics emerges above approximately 1 T, particularly at elevated temperatures above 20 K. This temperature-dependent divergence in J_c behaviour provides strong evidence for the increased effectiveness of flux pinning centers in the multilayer structures, especially at high temperatures [20], [22].

Comparing single-layer and multilayer films reveals that at lower BZO concentrations, the introduction of multilayering significantly increases $J_c(0)$. However, this enhancement diminishes progressively with increasing magnetic field. The most notable improvements due to multilayer architecture are found in the heavily doped samples, 8BZO and 10BZO, where the multilayer configurations consistently exhibit higher J_c values than their single-layer counterparts over the full temperature and field ranges examined. These findings align well with the structural improvements highlighted in the XRD analysis. As illustrated in Fig. 5, although M4 achieves the highest absolute J_c at high fields, the relative gain due to multilayering is comparatively modest. This leads to the conclusion that multilayering is most effective in enhancing J_c at high BZO concentrations. This is likely because increased BZO content introduces greater structural disorder, providing more scope for Ca-doping to counteract these defects and support improved crystalline quality.

C. Optimal BZO Doping Concentration in Various Magnetic Fields and Temperatures

The enhancements in J_c discussed in the previous section do not capture the complete picture. Although samples M8 and M10 exhibited the largest relative improvements, sample M4 consistently achieved the highest absolute J_c under most measurement conditions. As illustrated in Fig. 6, sample M0 yielded the highest J_c values at zero field and in low fields below 1 T across the entire temperature range. In contrast, within the intermediate field range of approximately 1 T to 2 T, particularly at elevated temperatures, sample M2 demonstrated the best performance. At magnetic fields exceeding 2 T, sample M4 clearly outperformed all others, delivering the highest absolute J_c throughout the full temperature range.

These findings suggest that at low magnetic fields, the improved crystalline quality and enhanced oxygenation, attributable to the Ca-doped spacer layer, are the dominant factors influencing J_c. However, as the magnetic field increases, flux pinning induced by BZO nanorods becomes increasingly important. There is, nevertheless, an optimal concentration threshold: excessive BZO content, as in samples M8 and M10, appears to deteriorate the YBCO matrix quality and ultimately compromises current-carrying performance.

D. Mechanism of Multilayering on Crystallinity and Flux Pinning

The lattice mismatch between BZO-nanorod and the surrounding YBCO matrix is around 7.7%. It has been shown that

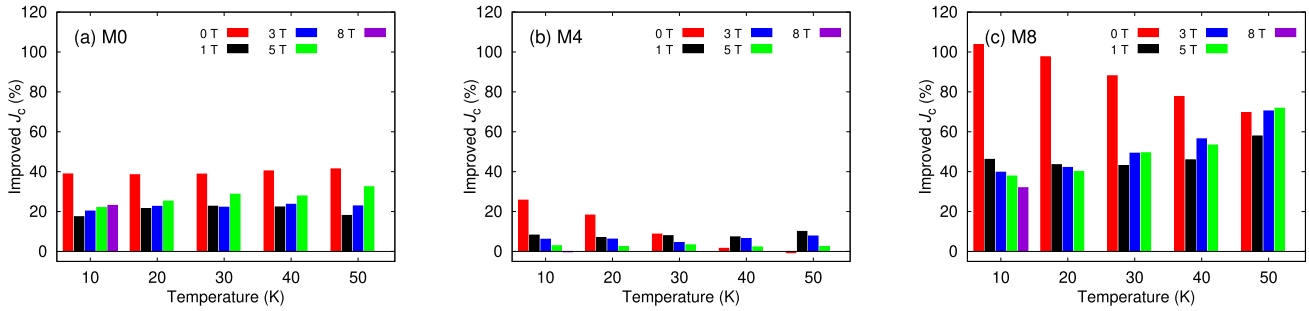

Fig. 5. Enhancement of J_c in multilayer films, (a) M0, (b) M4, and (c) M8, relative to single-layer films with corresponding BZO doping concentrations, measured over a wide range of temperatures and magnetic fields.

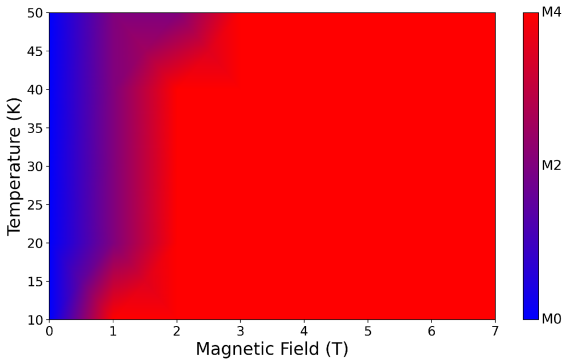

Fig. 6. Samples exhibiting the highest absolute J_c at various temperatures and magnetic fields, considering all single-layer and multilayer films.

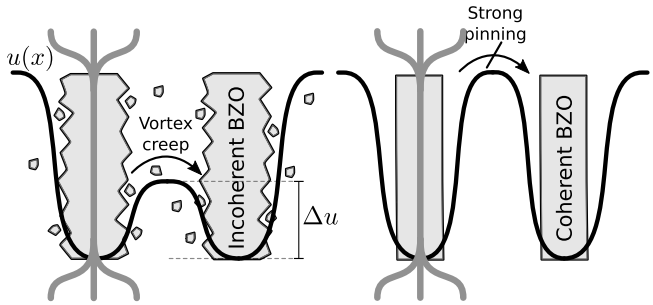

Fig. 7. A schematic illustration of how the coherence of the YBCO/BZO interface affects the hopping potential determining the creep rate.

the introduction of the Ca-spacer layers increases the length of the c-axis of YBCO and consequently reduces the lattice mismatch down to 1.4% [17], [28], [29]. The diffusion of Ca [17], [28] and oxygen [21], [26], [27], [30], [31], [32] (Section III-A) along with lattice mismatch related interface effects [21] have been proposed as the leading cause behind observation. To quantitatively discuss the resulting effects, we will adopt the model of critical thickness for the YBCO/BZO interface, defining the distance over which strain relaxes via the formation of dislocations. In the simplest approximation the critical thickness, here distance d_c from the YBCO/BZO interface along the surface of the film, is inversely proportional to the lattice mismatch f, that is $d_c \propto f^{-1}$ [33], [34]. In consequence, the Ca-spacer layer can decrease the d_c in multilayer samples (M) up to 5.5-fold ($d_{c,M}/d_{c,S} = f_S/f_M$) when compared with single films (S).

In our previous work [20], we have quantified the coherence of the YBCO/BZO interface via distance σ over which the value of superconducting order parameter increases from $\psi(x = 0) = 0$ to its maximum value (ideally $\psi(x = \sigma) = 1$), where $x = 0$ corresponds to the YBCO/BZO interface. In other words, σ represents the distance over which the dislocation density and strain measured from the nanorod interface decreases to a level corresponding to a homogeneous superconducting lattice. A sufficiently large σ results in the maximum $\psi < 1$ between the nanorods, which reduces the associated potential barrier Δu and thus favors vortex creep (see Fig. 7). As rigorously calculated in [20], $\Delta u(\sigma = 3.5\,\text{nm})/\Delta u(\sigma = 0) \approx 0.9$ and $\Delta u(\sigma = 7\,\text{nm})/\Delta u(\sigma = 0) \approx 0.7$ for a wide temperature range, suggesting a temperature independent non-linear decrease of Δu as a function of σ. Assuming that $\sigma \propto d_c$, i.e. the addition of Ca-spacer layer results in 5.5-fold decrease in σ, we can conclude that the effect of the spacer layer on the coherence of YBCO/BZO interface must be significant. Evidently, the effect is most prominent for the M8, where the spacing between the nanorods is smallest (Fig. 5(c)). The rather small improvement for M4 can be explained by the fact that the σ in the corresponding single layer films was already reasonably small, and consequently the main improvement in J_c comes solely from the improvement of $J_c(B = 0)$ resulting from reduced strain. This conclusion aligns with the observation (Fig. 5(b)–(c)) that the $J_c(B > 0)$ of M4 remains somewhat constant as a function of temperature, while for M8 increasing temperature dependence can be seen. The observed exponentially improved J_c as a function of temperature in Fig. 5(c) aligns well with the suggested model as the vortex creep rate is given by $\Gamma \propto \exp(-\Delta u/k_B T)$, where $\Delta u \propto d_c$. This can result in exponentially increasing creep rate as a function of temperature aligning with the observed trend for the improved $J_c(B > 0)$, together with the linearly decreasing $J_c(B = 0)$ for which vortex creep is absent.

IV. Conclusion

This work demonstrates that introducing a Ca-doped YBCO interlayer into BZO-doped YBCO multilayer structures significantly enhances the in-field critical current density across

a wide range of temperatures and magnetic fields. The Ca-doped layer improves structural quality, mitigates strain, and facilitates more uniform BZO nanorod growth, effects that become increasingly important at higher BZO concentrations. While the highest zero-field $J_c(0)$ is achieved in undoped multilayers, the optimal in-field performance is attained with 4% BZO doping at fields above 2 T, and 2% BZO near 1 T. These findings highlight the importance of combining controlled nanostructuring with compositional tuning to balance flux pinning and crystalline integrity. Such multilayer architectures offer a promising pathway for advancing the performance of YBCO-based coated conductors in real-world high-field applications.

REFERENCES

[1] M. Parizh, Y. Lvovsky, and M. Sumption, "Conductors for commercial MRI magnets beyond NbTi: Requirements and challenges," *Supercond. Sci. Technol.*, vol. 30, 2017, Art. no. 014007.

[2] X. Wang, S. A. Gourlay, and S. O. Prestemon, "Dipole magnets above 20 Tesla: Research needs for a path via high-temperature superconducting REBCO conductors," *Instruments*, vol. 3, 2019, Art. no. 62.

[3] N. Mitchell et al., "Superconductors for fusion: A roadmap," *Supercond. Sci. Technol.*, vol. 34, 2021, Art. no. 103001.

[4] A. Goyal et al., "Irradiation free, columnar defects comprised of self-assembled nanodots and nanorods resulting in strongly enhanced flux pinning in $YBa_2Cu_3O_{7-\delta}$ films," *Supercond. Sci. Technol.*, vol. 18, pp. 1533–1538, 2005.

[5] B. Maiorov et al., "Synergetic combination of different types of defect to optimize pinning landscape using $BaZrO_3$-doped $YBa_2Cu_3O_7$," *Nature Mater.*, vol. 8, pp. 398–404, 2009.

[6] R. L. S. Emergo, F. J. Baca, J. Z. Wu, T. J. Haugan, and P. N. Barnes, "The effect of thickness and substrate tilt on the BZO splay and superconducting properties of $YBa_2Cu_3O_{7-\delta}$ films," *Supercond. Sci. Technol.*, vol. 23, 2010, Art. no. 115010.

[7] S. Kang, K. J. Leonard, P. M. Martin, J. Li, and A. Goyal, "Strong enhancement of flux pinning in YBCO multilayers with columnar defects comprised of self-assembled BZO nanodots," *Supercond. Sci. Technol.*, vol. 20, pp. 11–15, 2007.

[8] J. Wu and J. Shi, "Interactive modeling-synthesis-characterization approach towards controllable in situ self-assembly of artificial pinning centers in RE-123 films," *Supercond. Sci. Technol.*, vol. 30, 2017, Art. no. 103002.

[9] I. A. Sadovskyy et al., "Toward superconducting critical current by design," *Adv. Mater.*, vol. 28, pp. 4593–4600, 2016.

[10] E. F. Talantsev and J. L. Tallon, "Universal self-field critical current for thin-film superconductors," *Nature Commun.*, vol. 6, 2015, Art. no. 7820.

[11] E. F. Talantsev, W. P. Crump, and J. L. Tallon, "Universal scaling of the self-field critical current in superconductors: From sub-nanometre to millimetre size," *Sci. Rep.*, vol. 7, 2017, Art. no. 10010.

[12] J. Z. Wu et al., "The effect of lattice strain on the diameter of $BaZrO_3$ nanorods in epitaxial $YBa_2Cu_3O_{7-\delta}$ films," *Supercond. Sci. Technol.*, vol. 27, 2014, Art. no. 044010.

[13] P. Paturi and H. Huhtinen, "Roles of electron mean free path and flux pinning in optimizing the critical current in YBCO superconductors," *Supercond. Sci. Technol.*, vol. 35, 2022, Art. no. 065007.

[14] G. Hammerl et al., "Enhanced supercurrent density in polycrystalline $YBa_2Cu_3O_{7-\delta}$ at 77k from calcium doping of grain boundaries," *Nature*, vol. 407, pp. 162–164, 2000.

[15] X. Song, G. Daniels, D. M. Feldmann, A. Gurevich, and D. Larbalestier, "Electromagnetic, atomic structure and chemistry changes induced by ca-doping of low-angle YBCO grain boundaries," *Nature Mater.*, vol. 4, pp. 470–475, 2005.

[16] A. V. Pan, S. V. Pysarenko, and S. X. Dou, "Drastic improvement of surface structure and current-carrying ability in $YBa_2Cu_3O_7$ films by introducing multilayered structure," *Appl. Phys. Lett.*, vol. 88, 2006, Art. no. 232506.

[17] V. Ogunjimi et al., "Enhancing magnetic pinning by $BaZrO_3$ nanorods forming coherent interface by strain-directed Ca-doping in $YBa_2Cu_3O_{7-x}$ nanocomposite films," *Supercond. Sci. Technol.*, vol. 34, 2021, Art. no. 104002.

[18] A. Tuomola, E. Rivasto, M. M. Aye, Y. Zhao, H. Huhtinen, and P. Paturi, "Defining optimal thickness for maximal self-field J_c in YBCO/CeO_2 multilayers grown on buffered metal," *J. Phys. Condens. Matter*, vol. 35, 2023, Art. no. 475001.

[19] E. Rivasto, M. Todorovic, H. Huhtinen, and P. Paturi, "Optimization of high-temperature superconducting multilayer films using artificial intelligence," *New J. Phys.*, vol. 25, 2023, Art. no. 113046.

[20] M. M. Aye, E. Rivasto, H. Huhtinen, and P. Paturi, "Enhanced critical current density in heterostructural YBCO/Ca-doped YBCO multilayers," *Cryst. Growth Des.*, vol. 24, pp. 4545–4555, 2024.

[21] M. M. Aye, E. Rivasto, H. Rijckaert, H. Huhtinen, and P. Paturi, "A method to enhance thickness and current-carrying capacity of BZO-doped YBCO multilayers," *IEEE T. Appl. Supercond.*, vol. 35, no. 5, Aug. 2025, Art. no. 6600506.

[22] M. Z. Khan et al., "Strongly enhanced growth of high-temperature superconducting films on an advanced metallic template," *Cryst. Growth Des.*, vol. 22, pp. 2097–2104, 2022.

[23] H. P. Wiesinger, F. M. Sauerzopf, and H. W. Weber, "On the calculation of J_c from magnetization measurements on superconductors," *Physica C*, vol. 203, pp. 121–128, 1992.

[24] B. D. Cullity and S. R. Stock, *Elements of X-Ray Diffraction*, 3 rd ed. Upper Saddle River, NJ, USA: Prentice Hall, 2001.

[25] M. Birkholz, *Thin Film Analysis by X-Ray Scattering*. Hoboken, NJ, USA: Wiley-VCH, 2006.

[26] J. L. Tallon et al., "Giant enhancement of oxygen mobility in high-T_c superconductors by atomic substitution," *Physica C*, vol. 171, pp. 61–68, 1990.

[27] J. T. Kucera and J. C. Bravman, "Transport characterization of calcium-doped YBCO thin films," *Phys. Rev. B*, vol. 51, pp. 8582–8590, 1995.

[28] M. A. Sebastian et al., "Impact of calcium doping of$YBa2Cu3O_{7-\delta}$ multilayer thin films on the flux pinning landscape at 65–5K, 0–9T for various applications," *IEEE Trans. Appl. Supercond.*, vol. 33, no. 5, Aug. 2023, Art. no. 8000606.

[29] A. K. Jha and K. Matsumoto, *Interfaces in REBCO-Based Nanocomposite Thin Films and Their Contribution to Vortex Pinning*, A. Roca, Ed. Berlin, Germany: Springer, 2021.

[30] Y. Zhao, H. K. Liu, and S. X. Dou, "Effect of co-doping of Ca and Al on hole concentration and superconductivity in the YBCO system," *Physica C*, vol. 179, pp. 207–213, 1991.

[31] C. Cantoni et al., "Strain-driven oxygen deficiency in self-assembled, nanostructured, composite oxide films," *ACS Nano*, vol. 5, pp. 4783–4789, 2011.

[32] T. Horide, K. Matsumoto, A. Ichinose, M. Mukaida, Y. Yoshida, and S. Horii, "Matching field effect of the vortices in $GdBa_2Cu_3O_{7-\delta}$ thin film with gold nanorods," *Supercond. Sci. Technol.*, vol. 20, 2007, Art. no. 303.

[33] J. W. Matthews and A. E. Blakeslee, "Defects in epitaxial multilayers: I misfit dislocations," *J. Cryst. Growth*, vol. 27, pp. 118–125, 1974.

[34] M. M. Aye, E. Rivasto, H. Rijckaert, H. Huhtinen, I. V. Driessche, and P. Paturi, "Controlled BZO nanorod growth and improved flux pinning in YBCO films grown on vicinal STO substrates," *Cryst. Growth Des.*, vol. 23, pp. 7971–7981, 2023.